Petroleum Science 21 (2024) 962–973

Contents lists available at ScienceDirect

Petroleum Science

journal homepage: www.keaipublishing.com/en/journals/petroleum-science

Original Paper

Study of deep transportation and plugging performance of deformable gel particles in porous media

Wen-Jing Zhao [a, b], Jing Wang [a, b, *], Zhong-Yang Qi [a, b], Hui-Qing Liu [a, b]

[a] National Key Laboratory of Petroleum Resources and Engineering, China University of Petroleum, Beijing, 102249, China
[b] MOE Key Laboratory of Petroleum Engineering, China University of Petroleum, Beijing, 102249, China

ARTICLE INFO

Article history:
Received 16 June 2023
Received in revised form
14 November 2023
Accepted 14 November 2023
Available online 18 November 2023

Edited by Yan-Hua Sun

Keywords:
Physical simulation
Deformable gel particle
Breakage
Particle size
Residual resistance coefficient

ABSTRACT

Deformable gel particles (DGPs) possess the capability of deep profile control and flooding. However, the deep migration behavior and plugging mechanism along their path remain unclear. Breakage, an inevitable phenomenon during particle migration, significantly impacts the deep plugging effect. Due to the complexity of the process, few studies have been conducted on this subject. In this paper, we conducted DGP flow experiments using a physical model of a multi-point sandpack under various injection rates and particle sizes. Particle size and concentration tests were performed at each measurement point to investigate the transportation behavior of particles in the deep part of the reservoir. The residual resistance coefficient and concentration changes along the porous media were combined to analyze the plugging performance of DGPs. Furthermore, the particle breakage along their path was revealed by analyzing the changes in particle size along the way. A mathematical model of breakage and concentration changes along the path was established. The results showed that the passage after breakage is a significant migration behavior of particles in porous media. The particles were reduced to less than half of their initial size at the front of the porous media. Breakage is an essential reason for the continuous decreases in particle concentration, size, and residual resistance coefficient. However, the particles can remain in porous media after breakage and play a significant role in deep plugging. Higher injection rates or larger particle sizes resulted in faster breakage along the injection direction, higher degrees of breakage, and faster decreases in residual resistance coefficient along the path. These conditions also led to a weaker deep plugging ability. Smaller particles were more evenly retained along the path, but more particles flowed out of the porous media, resulting in a poor deep plugging effect. The particle size is a function of particle size before injection, transport distance, and different injection parameters (injection rate or the diameter ratio of DGP to throat). Likewise, the particle concentration is a function of initial concentration, transport distance, and different injection parameters. These models can be utilized to optimize particle injection parameters, thereby achieving the goal of fine-tuning oil displacement.
© 2024 The Authors. Publishing services by Elsevier B.V. on behalf of KeAi Communications Co. Ltd. This is an open access article under the CC BY-NC-ND license (http://creativecommons.org/licenses/by-nc-nd/4.0/).

1. Introduction

Deformable gel particles (DGPs) were initially widely used in conventional reservoirs during the high water cut stages (Qiu et al., 2017). Excellent results with the use of DGP have been achieved in laboratory experiments (Bai et al., 2015; Imqam et al., 2018; Pi et al., 2023; Seidy Esfahlan et al., 2021) and field applications (Bai et al., 2007; Guo et al., 2022; Kang et al., 2021; Sang et al., 2014). As complex reservoirs transition into medium and high water cut stages, the demand for effective profile control intensifies. Concurrently, advancements in the preparation methods for DGP are emerging. DGP has been increasingly adopted for profile control in various challenging environments in response to these trends. These include fractured reservoirs (Imqam et al., 2015; Wang and Bai, 2018; Zhang et al., 2022; Zhao et al., 2021), high-salinity and high-temperature reservoirs (Wang et al., 2019; Wu et al., 2020; Yuan et al., 2021), and reservoirs with interlayer channels (Yang et al., 2021; Zhao et al., 2023b). Moreover, DGP is used to plug gas channeling during CO_2 flooding (Ji et al., 2023; Pu et al., 2021; Zhao et al., 2023a).

* Corresponding author. National Key Laboratory of Petroleum Resources and Engineering, China University of Petroleum, Beijing, 102249, China.
E-mail address: wangjing8510@163.com (J. Wang).

https://doi.org/10.1016/j.petsci.2023.11.016
1995-8226/© 2024 The Authors. Publishing services by Elsevier B.V. on behalf of KeAi Communications Co. Ltd. This is an open access article under the CC BY-NC-ND license (http://creativecommons.org/licenses/by-nc-nd/4.0/).

Abbreviation

DGP	Deformable gel particle
c_d	Concentration of the DGP suspension in the porous media
c_{d0}	Concentration of the DGP suspension before injection
d_d	Particle size of the DGP, μm
d_p	Pore diameter of the porous media, μm
d_{d0}	Particle diameter of DGP before injection, μm
F_{rrw}	Residual resistance coefficient
k	Permeability of the porous media, μm^2
ΔP_w	Pressure difference when conducting the water injection permeability test, Pa
ΔP	Pressure difference between each segment of the sandpack after DGP injection when conducting the water injection permeability test, Pa
ζ	Tortuosity of the porous media
ϕ	Porosity of the porous media
a, b	Constants related to the injection rate
c, d	Constants related to the diameter ratio of DGP to throat

DGP possesses the capacity to migrate within reservoirs, serving as an effective solution for deep profile control. It demonstrates superior application efficacy in complex reservoirs compared to other profile control agents, such as weak gels and foams. Nonetheless, successful deep profile control in such reservoirs relies heavily on a precise understanding of the transportation and plugging mechanisms of DGP. For instance, when employing DGP in reservoirs with interlayer channels, it is imperative to ascertain the DGP position in the reservoir to plug the channels effectively. This is critical to prevent the re-routing of subsequently injected water back through these channels (Yang et al., 2021). However, not all DGP are capable of deep transportation. Their ability to deep transportation is contingent upon compatibility with the pore size, elasticity, and the size of the DGP. Bai et al. (2013, 2007) suggested that effective particle transport in the pore throat occurs when the particle size is less than 5.71 times that of the pore throat. Elsharafi and Bai (2013) shows that DGP transportation will not happen when reservoir permeability falls below 320 mD or when the particle size to pore throat ratio exceeds 17. While researchers have managed to select DGP compatible with transportation in reservoirs, the law of DGP migration and plugging along the low path and deep within the reservoir remains poorly understood. Historically, researchers studied the plugging efficacy of DGP based on the pressure changes along the flow path (Yuan et al., 2021; Zhao et al., 2019), resistance coefficients of the entire physical model (Yao et al., 2013), and plugging efficiency (Imqam et al., 2018). Nevertheless, these methodologies have presented challenges in elucidating the transportation and plugging of DGP in the deep part of the reservoir.

Elucidating the behavior of DGP within deep reservoirs is pivotal for unraveling its transportation and plugging mechanisms. Several scholars have employed various visualization experiments, such as pore-throat models (Sang et al., 2014; Wang et al., 2012), mesoscale simulations (Wei et al., 2019; Zhou et al., 2017, 2019), and computational fluid dynamics (Feng et al., 2020; Wang et al., 2023) to study the behavior of DGP in the reservoir. Several types of behavior exhibited by DGP have been identified, including direct passage (Herterich et al., 2014), deformed passage, plugging retention, deposition retention, and breakage passage. The breakage law of DGP is not clear compared with the other four behaviors. Based on existing knowledge, a robust numerical simulation methodology has emerged (Farasat et al., 2021; Liu et al., 2017; Wang et al., 2013, 2017a, 2017b; Zhou et al., 2013), which has subsequently been applied within oilfields. It is acknowledged that the particle size distribution of DGP suspensions follows a lognormal pattern. Consequently, certain DGPs are incapable of direct or deformed passage and only break through under specific pressure gradients. Unveiling the breakage behavior of DGP is essential for enhancing their deep profile control effectiveness. Nevertheless, this DGP breakage presents considerable complexity (Liu et al., 2022). Some scholars have carried out research on the breakage of DGP, but it cannot not reflect the migration and breakage behavior of DGP in porous media. Feng et al. (2013) studied the breakage behavior of gel particles through multi-injection experiments. And they found that breakage only occurred near the injection well. However, Wang et al. (2017a, 2017b) obtained the criterion for particle breakage based on a pore-throat model, where the diameter ratio of DGP to throat (R) was more significant than 3. However, the breakage of DGP in porous media and deep parts of reservoirs has not yet been revealed.

This study used a physical model of a multi-point sandpack to conduct flow experiments of DGP under different injection rates and particle sizes. The changes in the residual resistance coefficient (F_{rrw}) along the flow path were calculated, and the plugging behavior of DGP in the deep porous media was investigated. Sampling experiments were carried out along the flow path to determine the changes in particle size and concentration under different injection rates and particle sizes, revealing the breakage pattern of DGP during transportation. An empirical function for the particle size and concentration of DGP at any position in the porous media was established, which is of significant guidance for determining breakage behavior, plugging strength, and injection parameter optimization of DPGs in deep parts of reservoirs.

2. Experimental

2.1. Experimental materials

The DGP used in this study was produced by Guangzhou Bofeng Chemical Technology Co., Ltd. As illustrated in Fig. 1, the DGP was a dry particle initially. The size of dry particles is 140–170 mesh. The change in particle size of DGP after water absorption and expansion

Fig. 1. Dry particles of DGPs.

is shown in Fig. 2(a). The particle size distribution after fully expanded is shown in Fig. 2(b). The DGP expanded 5.06 times after absorbing water for 12 h. After that, the particle size does not change. This paper does not study the effects of salt, so distilled water was used to prepare the DGP suspension and the displacement fluid. The physical model used in the sandpack was filled with quartz sand (10–20 mesh).

2.2. Experimental method and process

In this experiment, a sandpack model was used to simulate porous media. The sandpack had a length of 60 cm and a diameter of 3.8 cm, as shown in Fig. 3. In this paper, the transportation of DGPs in the dominant seepage channel of the reservoir in the high water cut stage is simulated by injecting DGPs into the sandpack. At every 15 cm of the sandpack, three interfaces were evenly distributed for pressure monitoring and sampling. The pressure measurement system employed a pressure sensor. A laser particle size analyzer (Mastersizer 3000) was used to measure particle size and concentration.

The experimental procedure, as shown in Fig. 4, involved simulating the flow of DGPs through a single sandpack. After injecting 15 pore volumes (PV) of DGPs, the F_{rrw} at different parts of the sandpack was measured. The stability of the pressure at each measurement point indicated the stability of the DGP transport and behavior (Wang et al., 2017a, 2017b). Therefore, the DGP suspension was further injected until the pressure at each measurement point stabilized after F_{rrw} testing. Samples were collected through the three interfaces along the sandpack to measure changes of particle size and concentration during the entire flow process. The injection rate and particle size (or the diameter ratio of DGP to the throat) were critical parameters that affected plugging and enhanced oil recovery (EOR) efficiency. Thus, this study investigated the effects of injection rate (Q) and the ration of diameter of DGP to throat (R) on the plugging and DGP transport mechanisms.

According to the experimental scheme, the parameters of sandpacks and DGPs were designed as shown in Table 1.

2.3. Experimental procedure

The experimental procedure is described as follows.

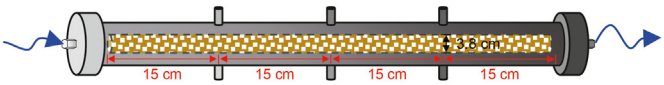

Fig. 3. The multi-point sandpack.

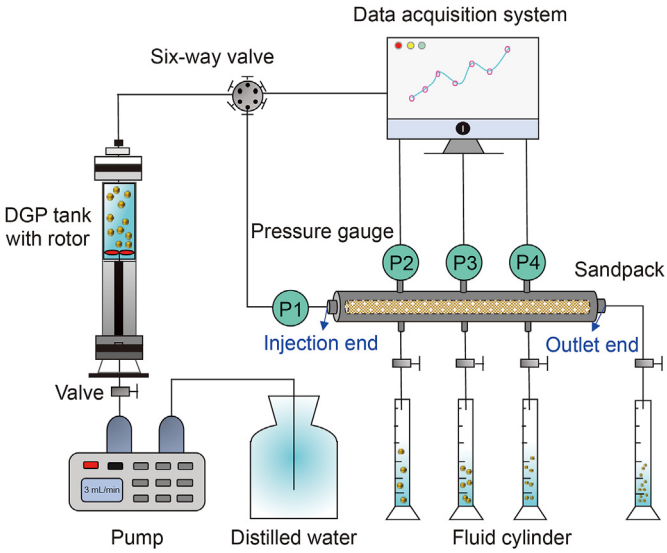

Fig. 4. The experimental flowchart of DGP transportation and plugging experiment.

(1) **Fabrication of a physical model of the sandpack**: The quartz sand is large enough that it can not flow out of the sampling interface and the sandpack. And the filter may affect the sampling results. Therefore, the filter was not used at the ends of the sandpack and the sampling interface. A filter was installed at the pressure measurement interface to prevent the pressure sensors from being blocked by DGPs. The sandpack was made using quartz sand. To avoid the influence of small sand adhering to the surface of the quartz sand on the analysis results of the extracted liquid, the sand was subjected to multiple screenings and repeated washing before filling.

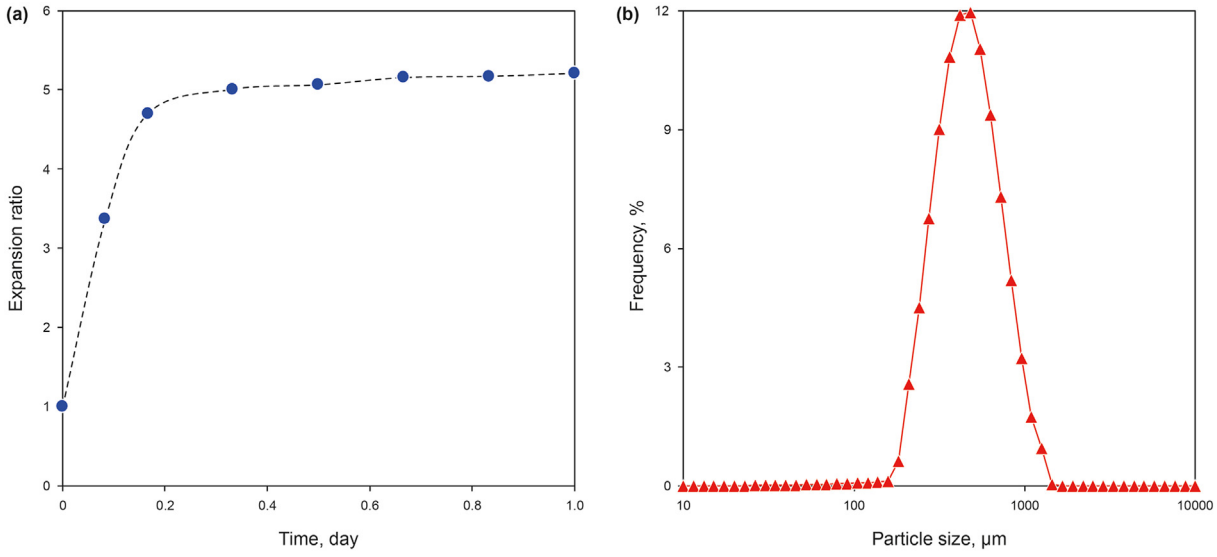

Fig. 2. (**a**) Swollen features of DGP; (**b**) Particle size distribution after swelling.

Table 1
Parameters of sandpacks and DGPs.

Exp. No.	Permeability, μm^2	Porosity	Injection rate, mL/min	Size of dry DGPs, mesh	Concentration of DGP suspension	d_{50} of DGPs after swelling, μm	Pore throat size, μm	Diameter ratio of DGP to throat
1	42.39	0.41	1	140–170	0.0936	512.33	172.56	2.97
2	41.87	0.32	3	140–170	0.0973	499.76	194.12	2.57
3	37.52	0.34	5	140–170	0.1032	507.45	178.27	2.85
4	40.13	0.30	3	100–140	0.0920	609.39	196.28	3.10
5	38.05	0.28	3	170–200	0.0988	353.39	197.83	1.79

(2) **Connection of experimental instruments**: The experimental setup was connected according to Fig. 4, and the air tightness was checked. To prevent precipitation of the DGP suspension, a magnetic stirring device was installed in the tank of DGPs.

(3) **Sandpack property testing:** The sandpack was saturated with distilled water at an injection rate of 0.5 mL/min. The porosity of sandpack can be obtained according to the volume of saturated water. Then, the distilled water was injected into the sandpack at 3 mL/min. The permeability of the sandpack was calculated using Darcy's law according to the stabilized pressure. The pressure sensors (measurement range of 0–10 kPa) were used to monitor pressure changes in this step. Then, the pore throat size of the porous media is obtained using the Kozeny–Carman equation (Wang et al., 2013):

$$d_p = \sqrt{\frac{32\varsigma^2 k}{\phi}}, \tag{1}$$

where ς represents tortuosity (1.5–5), which is 3 in this paper; k is the permeability of the porous media, μm^2; ϕ is the porosity of the porous media.

The expression for the diameter ratio of DGP to the throat is

$$R = \frac{d_{d0}}{d_p}, \tag{2}$$

where d_{d0} is the particle size of DGP before injection, μm; d_p is the pore diameter of the porous media, μm.

(4) **DGP injection:** The DGP suspension was injected with the parameters according to Table 1. The experiment was stopped when the pressure was stable and the cumulative injection volume reached 15 PV.

(5) **Residual resistance coefficient (F_{rrw}) test**: The distilled water was injected at an injection rate of 3 mL/min, the same as during permeability testing after the DGP injection. The F_{rrw} along the injection direction and the F_{rrw} of the whole sandpack were calculated according to the stabilized pressure of each measurement point. And the expression of F_{rrw} is given by

$$F_{rrw} = \frac{\Delta P}{\Delta P_w}, \tag{3}$$

where F_{rrw} is the residual resistance coefficient of the sandpack; ΔP_w is the pressure difference of each part of the sandpack measured by constant rate water injection before DGP injection, Pa; ΔP is the pressure difference of each section of the sandpack at the same rate of water injection after DGP injection, Pa.

(6) **Sampling and testing along the sandpack**: The DGP suspension was continuously injected until the pressure at each measurement point was stable. And after 15 PV of DGP suspension had been injected, the injection process was stopped. Then, the outlet of the sandpack was closed. To avoid any undue influence on subsequent parts of the sandpack. The first sampling port along the injection direction was opened. After taking out the fluid of 1 PV, the sampling port was closed, and the next sampling port along the injection direction was opened. This process was repeated for the three sampling ports and the outlet. Particle size and concentration tests were performed on the collected fluid from each sampling port and outlet.

3. Experimental results

3.1. Deep plugging performance of DGPs

3.1.1. Effect of injection rate on plugging

The pressure changes at each measurement point obtained during the DGP injection are shown in Fig. 5. It can be observed that the pressures at all measurement points tend to stabilize after rising under every injection rate. The degree of pressure fluctuation varies among these points, especially during the pressure-rising stage. This phenomenon is attributed to the differential behavior of DGPs in different parts of the sandpack, where more frequent breakage-remobilization and deformation-remobilization occur in the front part. As a result, the higher the injection rate is, the higher the pressure at the injection end is, and the more obvious the pressure fluctuation at each point is. The steady injection pressure reaches 4.55 MPa when the injection rate is 5 mL/min, and the maximum pressure fluctuation in the injection process is 1.6 MPa. After pressure stabilization, the pressure difference of each part of the sandpack can be characterized to represent, to some extent, the migration behavior of DGP in porous media. As shown in Fig. 5, the pressure difference of the first part of the sandpack is the largest at different injection rates. The pressure difference of the last three parts of the sandpack is basically similar. The breakage behavior of DGPs is most pronounced in the first part.

Consequently, the pressure difference in the first part exceeds that of other parts by more than 1.19 times, except when subjected to an injection rate of 3 mL/min. Under an injection rate of 3 mL/min, due to the extensive bridging of transported particles, a pressure difference of 1.41 MPa is observed, which surpasses the 1.04 MPa of the first part. It has been identified by Zhao and Bai (2022) that the pressure difference closer to the outlet end of the porous media exceeds that near the injection end. An increase in injection rate is associated with a heightened degree of breakage. Therefore, when injecting DGP suspension at a high rate, the pressure difference between the middle two parts of the sandpack is small. In the latter half, the likelihood of particle collisions, either interparticle or with pores, increases. As a result, as the injection rate rises, a significant pressure difference is observed in the half part of the sandpack. Nonetheless, the subsequent water injection is minimally influenced by broken DGPs. Therefore, high-rate injection of DGP suspension does not result in a substantial F_{rrw} in the

more significant part of the pressure difference.

The residual resistance coefficient (F_{rrw}) is an essential parameter for evaluating the effectiveness of DGP. Although previous studies have obtained the pressure gradient of each part of the physical model (Imqam et al., 2018), the F_{rrw} of the entire physical model is usually measured, neglecting the plugging capacity of DGP in the deeper part. Firstly, the traditional method is used to calculate the F_{rrw} of the entire sandpack based on the pressure difference between the injection and outlet ends (Table 2). The calculation results are shown in Fig. 6(a). The F_{rrw} of the entire sandpack decreases with the injection rate increasing, consistent with the existing literature (Song et al., 2018). However, the variation trend of the F_{rrw} in different parts of the sandpack is different.

Then, the F_{rrw} of each part of the sandpack is calculated according to the pressure difference of each part (Table 2). As shown in Fig. 6(b), the calculated F_{rrw} of each segment is used as the F_{rrw} at the midpoint of each part to obtain the relation between the F_{rrw} and the dimensionless distance of DGP transportation. The fluctuations observed in the F_{rrw} at each injection rate conform to an exponential function. Furthermore, it is noteworthy that the calculated results exhibit remarkable agreement with the experimental results. Due to the filtration and breakage of DGPs, the plugging effect weakens along the injection direction. Therefore, the F_{rrw} decreases exponentially along the injection direction at each injection rate. The higher the injection rate, the faster the F_{rrw} decreases along the injection direction in each part of the sandpack. At an injection velocity of 5 mL/min, the F_{rrw} of the first part is higher than other parts of the sandpack. And it decreases rapidly to 58.48 and then tends to be stable.

3.1.2. Effect of the diameter ratio of DGP to throat on plugging

The variations in pressure at different measurement points under the influence of the diameter ratio of DGP to the throat during the flow experiment are shown in Fig. 7. The diameter ratio of DGP to throat has a significant impact on the injection pressure, as smaller ratios result in a delay in pressure stabilization at each measurement point. When the diameter ratio of DGP to throat is 1.79, the pressure of each part of 13.46 PV is stable after DGP injection. In contrast, the pressure is stable when it reaches 9.89 PV, under the ratio of 3.10. The maximum injection pressure of small DGP is the minimum owing to the diminished plugging strength. Specifically, at the diameter ratio of DGP to throat of 1.79, the maximum pressure reaches merely 0.56 times that observed at a ratio of 3.10.

When confronted with a relatively large diameter ratio of DGP to the throat, severe breakage behavior is observed at the front end of the sandpack. Consequently, with a diameter ratio of DGP to throat of 3.10, a pressure difference of 1.40 MPa in the first part exceeds that of other diameter ratios. As the diameter ratio of DGP to the throat diminishes, few DGPs undergo breakage and pass through the throat directly. As a result, the pressure difference across each part consistently diminishes, presenting values lesser than those observed for other injection particle sizes. The pressure difference in the terminal section constitutes merely 0.08% of the value of the first part. In the subsequent three parts, fragments produced by DGPs of a larger particle size are either obstructed or subjected to further breakage. Nevertheless, this effect progressively diminishes until the pressure difference in the final section reduces to 0.79 MPa.

The F_{rrw} under varying diameter ratios of DGP to throat based on the pressure difference shown in Table 3 was calculated using the methodology delineated in the preceding section. The calculated results are depicted in Fig. 8. The F_{rrw} of the entire sandpack is maximum when the diameter ratio of DGP to the throat is 2.57. Both excessively large and small particle sizes can cause a rapid decrease in the F_{rrw} along the flow path. As shown in Fig. 8(b), The variation pattern of F_{rrw} mirrors that observed under varying DGP injection rates. Specifically, as different diameter ratios of DGP to throat are considered, the F_{rrw} exhibits an exponential decline in response to increasing migration distances. In the initial stages of DGP injection, an excessively large diameter ratio of DGP to the throat can cause smaller particles in the DGP suspension system to enter the sandpack.

In comparison, a more significant number of larger particles also plug at the inlet. As injection pressure increases, the particles plugging at the inlet break down and enter the porous media. Furthermore, the broken DGP fails to create effective plugging. On the other hand, when the diameter ratio of DGP to the throat is too small, effective plugging cannot be achieved at the inlet, and most small particles in the DGP suspension system enter the porous media directly. Consequently, the F_{rrw} for both diameter ratios of DGP to the throat is relatively low at deeper points in the porous media.

3.2. Deep transportation of deformable gel particles

The concentration and particle size are the two most critical factors that affect the effectiveness of the DGP in the deep part of the reservoir and are also critical parameters in the numerical simulation of particle placement. The particle size in the reservoir can be divided into two types: the particle size of the DGPs trapped in the pore throat, and the particle size of the DGPs which can be transported through the pore throat. Similarly, the concentration can be divided into the concentration of the DGPs trapped in the pore throat and the concentration of the DGPs which can be transported through the pore throat, with the sum of these two concentrations being the injection concentration. As shown in Fig. 9(a), the change in particle size along the transport path was obtained by comparing the particle size obtained at each measurement point with the particle size before injection. The independent variable (abscissa) is the dimensionless distance, which is the ratio of the transport distance of the particles in the sandpack to the length of the sandpack. Similarly, as shown in Fig. 9(b), the change in concentration along the path was obtained by comparing the concentration of the suspended particles with the concentration before injection and the relation between the dimensionless distance and the concentration change was established.

Breakage is often overlooked by scholars. And it represents a distinct type of DGP transportation behavior. Upon examination of the particle size distribution curves influenced by various factors, as illustrated in Fig. 10, several observations emerge. The left end of the particle size distribution curve, aligned with the DGP transportation direction, shifts towards zero. This curve displays a diminishing intersection with the particle size distribution curve of DGP before injection. It shows that more small particles that do not exist before injection are generated. Such small particles are discerned as breakage formed during the DGP transport. The intersecting part of the particle size distribution curve along the route and the part before injection is the DGP passed directly or deformed. The DGP of this part decreases gradually with the transport of particles. For example, when the injection rate is 3 mL/min, the minimum particle size decreases from 26.30 μm before injection to 0.03 μm at the outlet end. Correspondingly, the overlap with the particle size distribution curve before injection decreases from (69.18, 1181.97 μm) to (26.30, 1096.478 μm). In summary, passing after breaking is the main form of DGP migration in the deep porous media.

The size and concentration of DGPs that can be transported through the pore throat are obtained through the sampling experiment. The concentration of the DGPs trapped in the pore

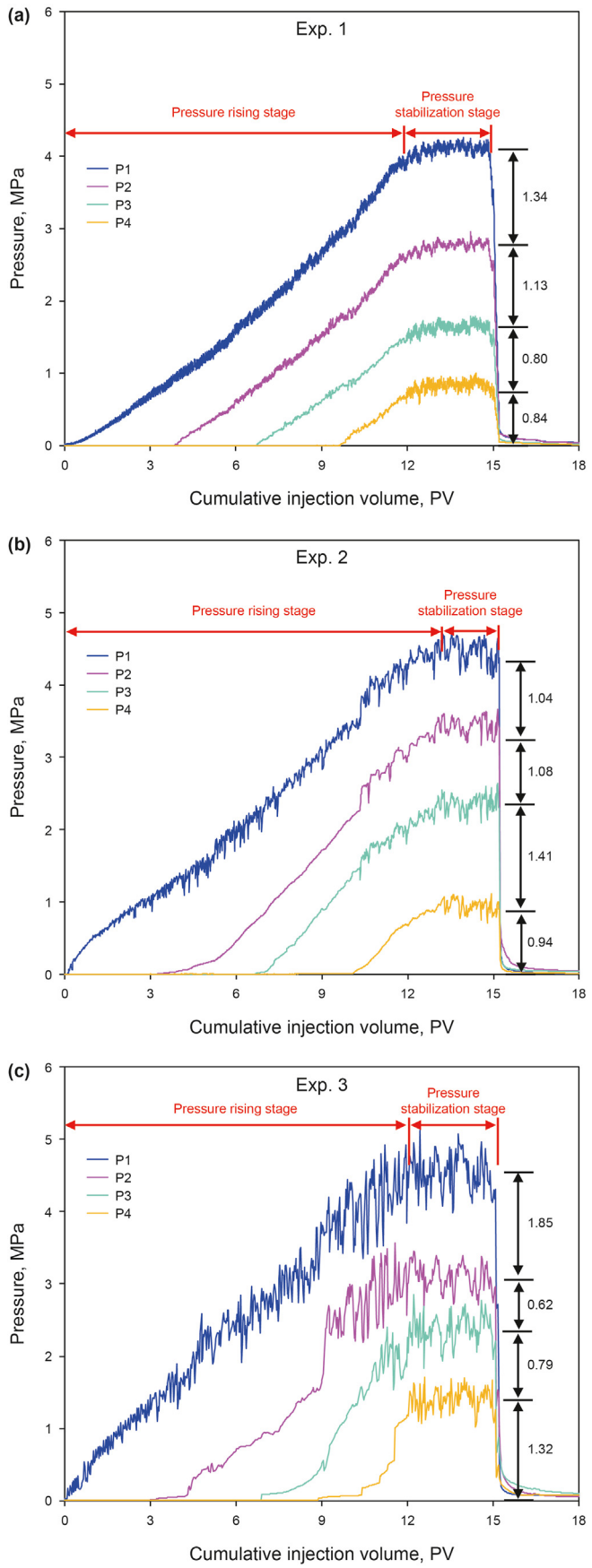

throat between two locations can be characterized by the difference in concentration between the two locations. A rapid decrease in concentration indicates that particles are trapped more in the earlier stages of the transport process. A more uniform change in concentration indicates that particles are trapped more evenly along the transport path. A higher retention concentration indicates that more particles act between the two locations, resulting in better plugging effects. The sustained decrease in the concentration of broken particles indicates that these particles can also be trapped in the deep porous media when encountering pore throats smaller than their size, thus achieving a deep plugging effect. Analysis of the particle size change under different factors shows that larger particles are constantly plugged and retained after filtration along the flow direction. Therefore, the DGP suspension concentration decreases with an increase in the transport distance under different injection rates and diameter ratios of DGP to the throat.

The transport law of DGP in porous media can be obtained by combining the particle size distribution curve with the variation of median particle size (d_{50}) and concentration. And the difference of F_{rrw} mentioned in the previous section can also be explained. The detailed analysis of the transportation law of DGP under the influence of various factors is as follows.

3.2.1. Effect of injection rate on the DGP transportation

The DGP transportation law under different injection rates can be obtained combined with the particle size distribution curve of the produced liquid in Fig. 10. The pressure at the injection end is higher than other positions of the sandpack under different DGP injection rates. So, the breakage and deformation of DGP in the front of the sandpack are the most violent. The decrease rates of particle size and concentration in the front of the sandpack are the fastest. Therefore, as shown in Fig. 9, the changes in particle size and concentration are in accordance with the exponential function. The higher the injection rate is, the more severe the breakage behavior is, the faster the DGP particle size decreases. Especially when the injection speed is 5 mL/min, the particle size becomes 0.11 times that before injection when the DGP transports to 1/4 of the sandpack. And the double peaks of the particle size distribution curve are formed (Fig. 10(c)). The broken particles transport in the porous media, resulting in high concentration in the suspension. However, at a low injection rate, the weaker injection intensity leads to the minor breakage behavior of DGP, so the particle size decreases slowly. When the injection rate is the lowest, and the dimensionless transport distance of DGP is 0.25, the particle size decreases to 0.47 times before injection. By analyzing the particle size distribution curve, it can be found that the higher the injection rate, the more concentrated the particle size of each part. In other words, the higher the injection rate, the smaller the particle size distribution range and the fewer peaks. The lower flow velocity also increases the collision contact probability between DGP and the pore throat, which makes it easier for particles to be deposited in the pore throat by gravity. Therefore, the suspension concentration decreases rapidly when the injection rate is 1 mL/min. Moreover, 99.46% of the volume of DGP was trapped in porous media before injection, which was higher than 97.36% at 5 mL/min. Therefore, the F_{rrw} of the front half of the sandpack is higher under a low DGP injection rate (Fig. 6).

The relation between the particle diameter d_{d1}, concentration c_{d1}, and the migration distance x of DGP and the particle diameter d_{d0} before injection can be expressed by the exponential function

Fig. 5. Pressure change at each point of the sandpack under different injection rates. (**a**) $Q = 1$ mL/min; (**b**) $Q = 3$ mL/min; (**c**) $Q = 5$ mL/min.

Table 2
Pressure difference during F_{rrw} testing after DGP injection at different injection rates.

Exp. No.	Injection rate, mL/min	Stable pressure, MPa			
		Part 1	Part 2	Part 3	Part 4
1	1	104.21	15.21	14.66	13.93
2	3	93.07	30.97	25.07	13.77
3	5	97.47	53.41	23.01	13.53

Table 3
Pressure difference during F_{rrw} testing after DGP injection in different diameter ratios of DGP to throat.

Exp. No.	Diameter ratio of DGP to throat	Stable pressure, MPa			
		Part 1	Part 2	Part 3	Part 4
4	3.10	101.72	22.70	15.48	13.08
2	2.57	93.07	30.97	25.07	13.77
5	1.79	82.76	30.49	14.56	13.35

shown in Eq. (4). Similarly, the concentration c_d and migration distance x of DGP, as well as the initial concentration c_{d0} of the DGP suspension before injection, exhibit an exponential function relation as shown in Eq. (5):

$$d_{d1} = d_{d0}e^{ax}, \tag{4}$$

$$c_{d1} = c_{d0}e^{bx}, \tag{5}$$

where d_{d0} represents the particle diameter of DGPs before injection; c_d represents the concentration of the DGP suspension in the porous media; c_{d0} represents the concentration of the DGP suspension before injection; a and b are constant related to the injection rate.

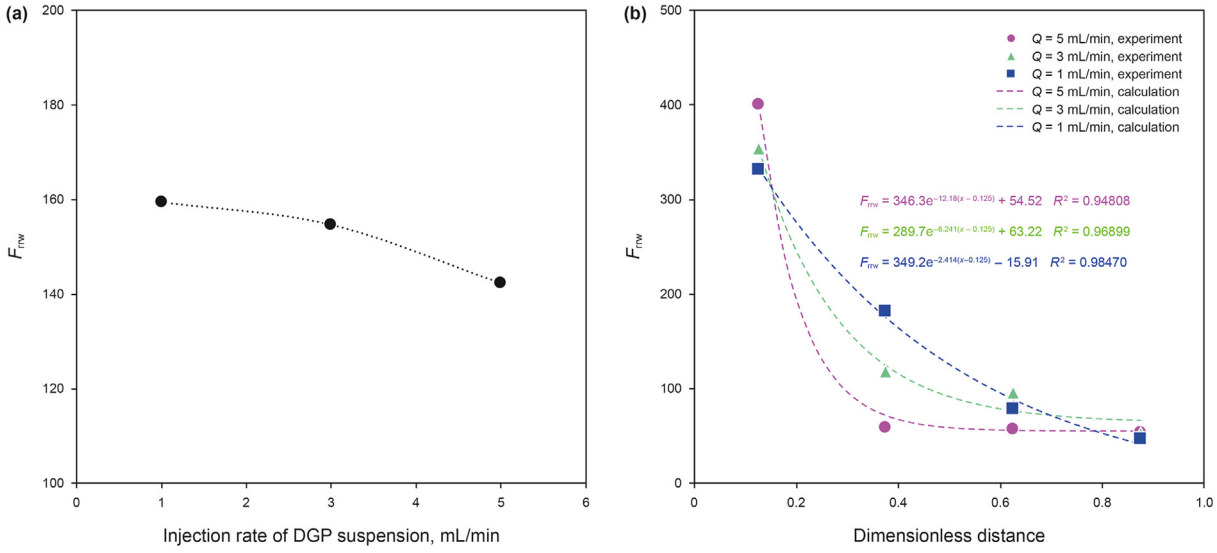

Fig. 6. (**a**) Effect of the injection rate of DGP suspension on F_{rrw}; (**b**) F_{rrw} of each segment of the sandpack along the flow path.

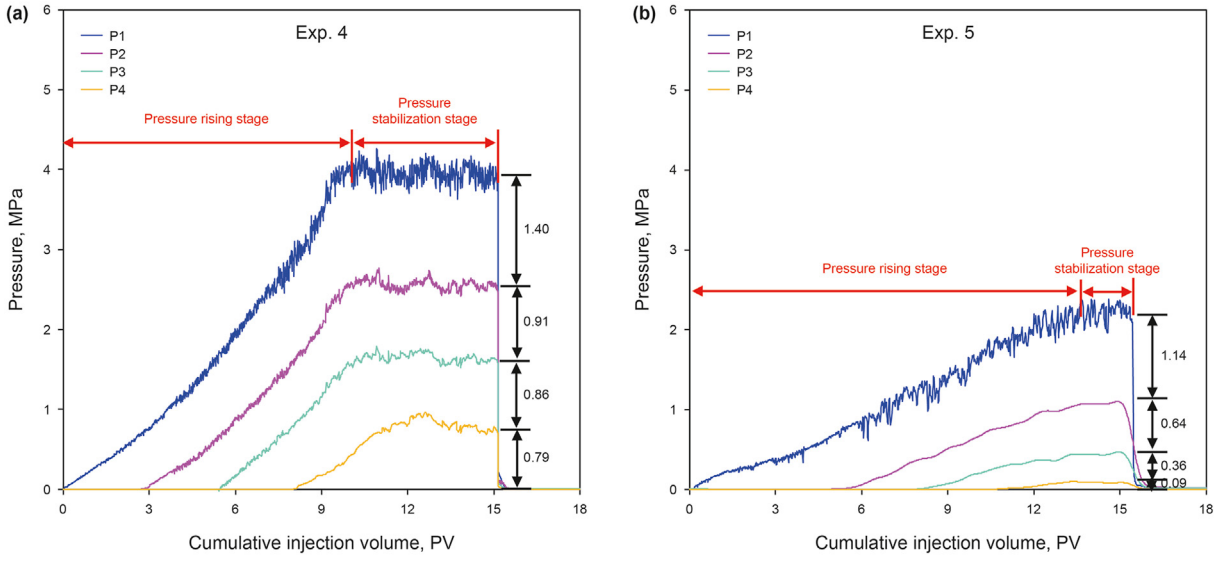

Fig. 7. Pressure change at each part of the sandpack under the influence of different diameter ratios of DGP to the throat. (**a**) $R = 3.10$; (**b**) $R = 1.79$.

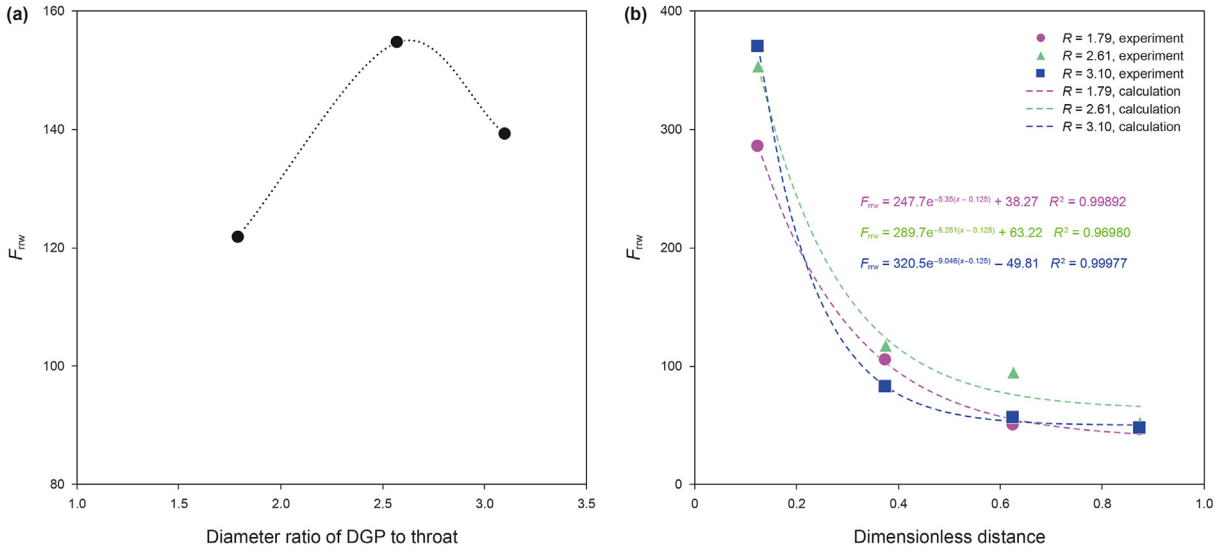

Fig. 8. (**a**) Effect of diameter ratio of DGP suspension to throat on F_{rrw}; (**b**) F_{rrw} of each segment of the sandpack along the flow path.

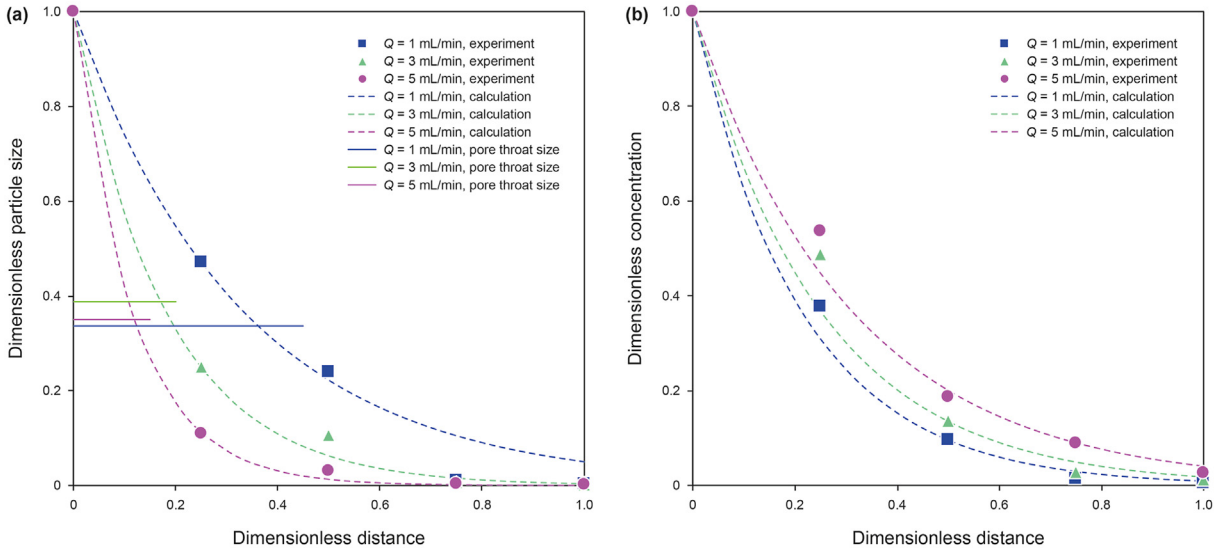

Fig. 9. Effect of injection rate of DGP on particle size (**a**) and concentration (**b**) along the flow path.

Table 4 shows the fitted relations between the particle size of DGP and the migration distance, as well as the suspension concentration of DGP and the migration distance at different injection rates. The fitting degree (R^2) can reach more than 0.98, indicating that the fitting effect is good, and the fitting function can reflect the change of particle size and concentration of DGP in the sandpack. As shown in Fig. 11, the coefficients a and b in the function vary linearly with the increase in injection rate.

The relation between DGP particle size and injection rate, particle size before injection, and transport distance can be obtained by substituting the relationship between a and injection rate into Eq. (4):

$$d_{d1} = d_{d0}e^{(-1.4173Q-1.4919)x}. \quad (6)$$

Similarly, the relation between DGP suspension concentration and injection rate, particle size before injection, and transport distance can be obtained by substituting the relationship between a and injection rate into Eq. (5):

$$c_{d1} = c_{d0}e^{(0.3685Q-5.0685)x}. \quad (7)$$

3.2.2. Effect of the diameter ratio of DGP to throat on transportation

Experimental results (Fig. 12) show that when the diameter ratio of DGP to throat is large, more particles experience breakage under higher injection pressures, resulting in smaller ratios of broken particle size to particle size before injection, thus leading to the fastest reduction in particle size. The intersection of the particle size distribution curve at each position and before injection is less than the other diameter ratio of DGP to throat compared with smaller ratio of particle size to pore throat. The larger the diameter ratio of DGP to throat is, the more obvious the main peak of the particle size distribution curve along the transport direction is (Fig. 13). However, many particles still cannot enter the porous

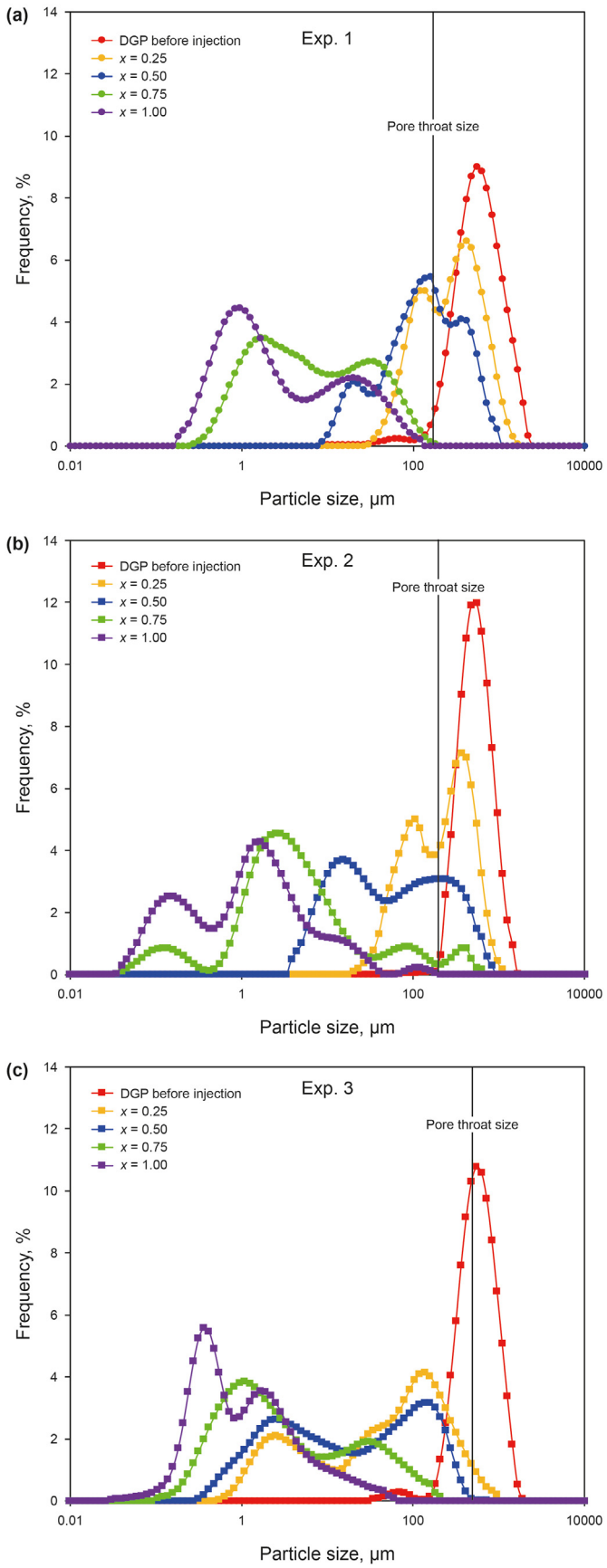

media under the existing injection pressure. They can only be retained and blocked in the front end, causing a rapid decrease in concentration at the front end when the diameter ratio of DGP to throat is 3.10. And the concentration decreases to 21.97% before injection when DGP transport to 1/4 of the sandpack. It can explain why the F_{rrw} decreases rapidly when the diameter ratio of DGP to throat is large. When the diameter ratio of DGP to throat is small due to the smaller number of large particles in the DGP system, the injection pressure rises more slowly, and deformation and breakage begin slowly with increasing pressure. Therefore, the breakage behavior of DGP is less, and mainly, the small particles in the system pass through directly when the diameter ratio of DGP to throat is 1.79, which makes the particle size decrease the slowest. And the particle size is reduced to 18.34% when DGP transported to half of the sandpack, which is much higher than the 7% when the diameter ratio of DGP to throat is 3.10. Some small particles are in the DGP system before injection flows out from the sandpack. So, the particle size distribution curve of the outlet-produced liquid still intersects with the particle size distribution curve before injection (Fig. 13(a)).

However, in DGP systems with smaller particle sizes, more particles flow out at the outlet, resulting in minor total retention. Therefore, when the diameter ratio of DGP to throat is 1.79, the total retention of DGP in porous media is the smallest. And 90.02% of the volume of DGP before injection is blocked in the sandpack. So, under the diameter ratio of DGP to throat of 1.79, the F_{rrw} is the smallest, especially in the middle and rear of the sandpack (Fig. 8). Like the relation between particle size, concentration, and transport distance under different injection rates, the relation between the diameter ratio of DGP to throat also shows an exponential relation:

$$d_{d2} = d_{d0}e^{cx}, \tag{8}$$

$$c_{d2} = c_{d0}e^{dx}. \tag{9}$$

The relations between particle size and transport distance and particle suspension concentration and transport distance were obtained through fitting at different diameter ratios of DGP to throat, as shown in Table 5. The fitting results were satisfactory; all coefficients showed linear relations with the diameter ratio of DGP to throat (Fig. 14).

By substituting coefficients e and f with the diameter ratio of DGP to throat into Eqs. (8) and (9), respectively, the relationships between particle size and the diameter ratio of DGP to throat, particle size before injection, and transport distance were obtained

$$d_{d2} = d_{d0}e^{(-4.3867R+4.8479)x}. \tag{10}$$

Similarly, the relationships between DGP suspension concentration and the diameter ratio of DGP to throat, particle size before injection, and transport distance were obtained

$$c_{d2} = c_{d0}e^{(-3.0753R+3.6885)x}. \tag{11}$$

Eqs. (6), (7), (10) and (11) are of great significance for determining the particle size attenuation of deformable particles and for the breakage dynamics model in numerical simulation.

4. Conclusions

This study used a sandpack with multi-point to investigate the

Fig. 10. Effect of diameter ratio of DGP to throat on particle size distribution along the flow path (x is the dimensionless migration distance). (**a**) $Q = 1$ mL/min; (**b**) $Q = 3$ mL/min; (**c**) $Q = 5$ mL/min.

Table 4
Fitting equations for particle size and concentration at different injection rates as a function of the injection rate and the transport distance.

Dependent variable	Injection rate, mL/min	a	b	Fitting equation	R^2
Particle size	1	−3.014		$d_{d1} = d_{d0}e^{-3.014x}$	0.9835
	3	−5.534		$d_{d1} = d_{d0}e^{-5.534x}$	0.9990
	5	−8.683		$d_{d1} = d_{d0}e^{-8.683x}$	0.9995
Concentration	1		−3.212	$c_{d1} = c_{d0}e^{-3.212x}$	0.9943
	3		−3.991	$c_{d1} = c_{d0}e^{-3.991x}$	0.9948
	5		−4.686	$c_{d1} = c_{d0}e^{-4.686x}$	0.9908

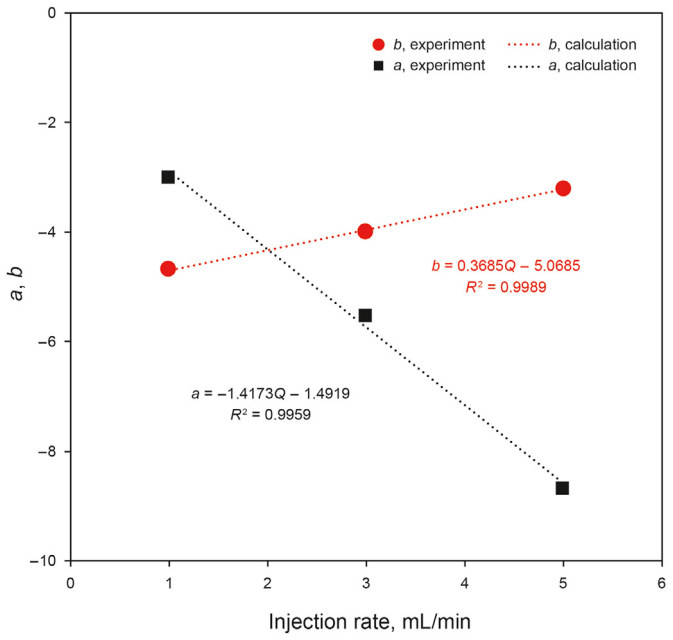

Fig. 11. The relationship between coefficients a, b and injection rate.

plugging and transportation behavior of DGPs in the deep parts of the reservoirs. The F_{rrw}, concentration, and particle size changes along the flow path were obtained, leading to the following conclusions.

(1) Breakage is one of the main transport behavior of DGP in porous media. The particle size can be reduced to 0.7% of the particle size before injection when the DGP transport to half the length of porous media because of DGP breaking. And the breakage leads to the exponential decrease of the residual resistance coefficient (F_{rrw}) along the flow way.
(2) The higher the injection rate, the more intense the breakage in the front of the porous media and the lower the concentration of particles retained in the pores, resulting in poorer plugging effects in the deep parts. The larger the diameter ratio of DGP to throat, the higher the breakage degree of DGP is, and the easier it is to remain in the front of the porous media.
(3) Optimal plugging efficacy is attained when DGP is injected with a particle size commensurate with the pore size. The deep plugging effect is the best when the diameter ratio of DGP to throat is 1.79. Breakage of DGP is mitigated by low-rate injection. Consequently, DGP should be injected at a low rate as much as possible.
(4) The concentration change along the flow path is an exponential function of the transport distance, initial concentration, and injection parameters (injection rate and the diameter ratio of DGP to throat). In contrast, the particle size change along the flow path is an exponential function of the transport distance, particle size before injection, and injection parameters. The model of particle size and concentration change along the flow path can be used to optimize the

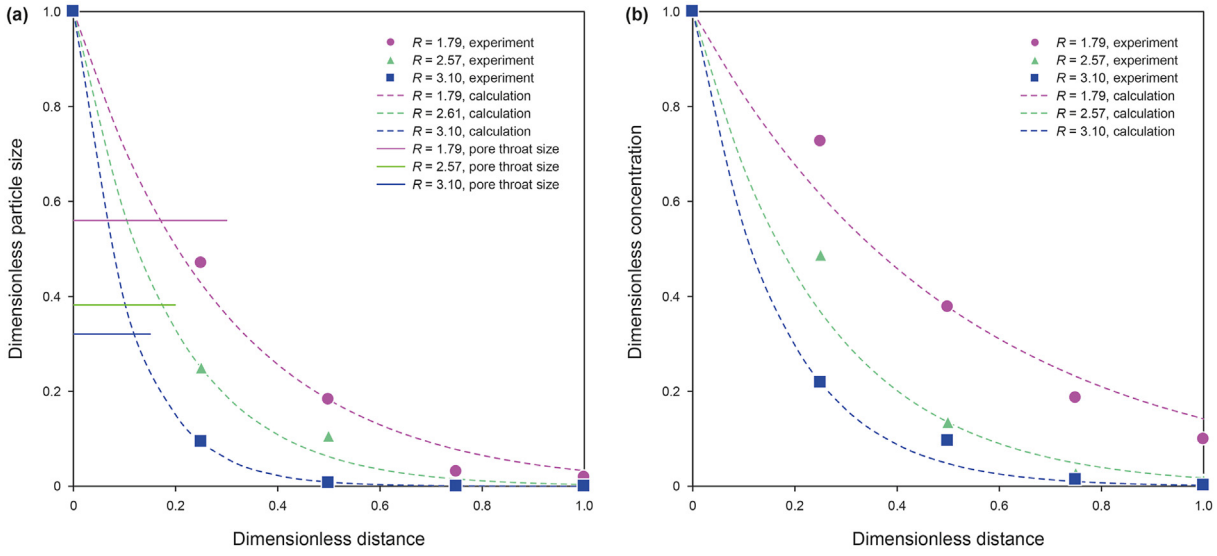

Fig. 12. Effect of diameter ratio of DGP to throat on particle size (**a**) and concentration (**b**) along the flow path.

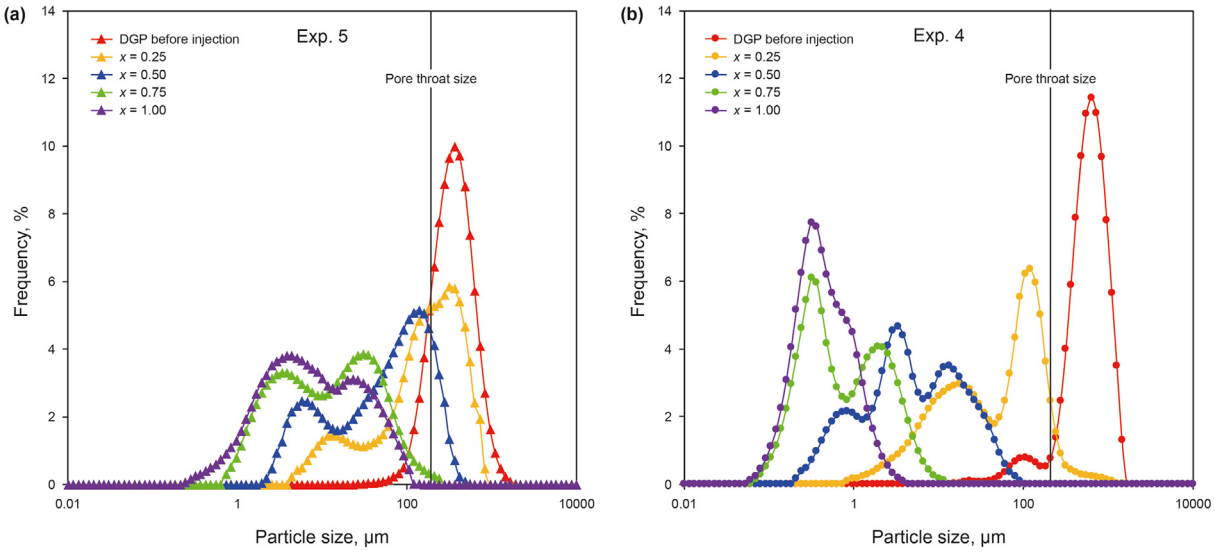

Fig. 13. Effect of diameter ratio of DGP to throat on particle size distribution along the flow path. (**a**) $R = 1.79$; (**b**) $R = 3.10$.

Table 5
Fitting equations for particle size and concentration at different diameter ratios of DGP to throat as a function of the diameter ratio of DGP to throat and the transport distance.

Dependent variable	Diameter ratio of DGP to throat	c	d	Fitting equation	R^2
Particle size	1.79	−3.392		$d_{d2} = d_{d0}e^{-3.392x}$	0.9937
	2.57	−5.534		$d_{d2} = d_{d0}e^{-5.534x}$	0.9989
	3.10	−9.453		$d_{d2} = d_{d0}e^{-9.453x}$	0.9999
Concentration	1.79		−1.946	$c_{d2} = c_{d0}e^{-1.946x}$	0.97084
	2.57		−3.991	$c_{d2} = c_{d0}e^{-3.9991x}$	0.99477
	3.10		−6.062	$c_{d2} = c_{d0}e^{-6.062x}$	0.99874

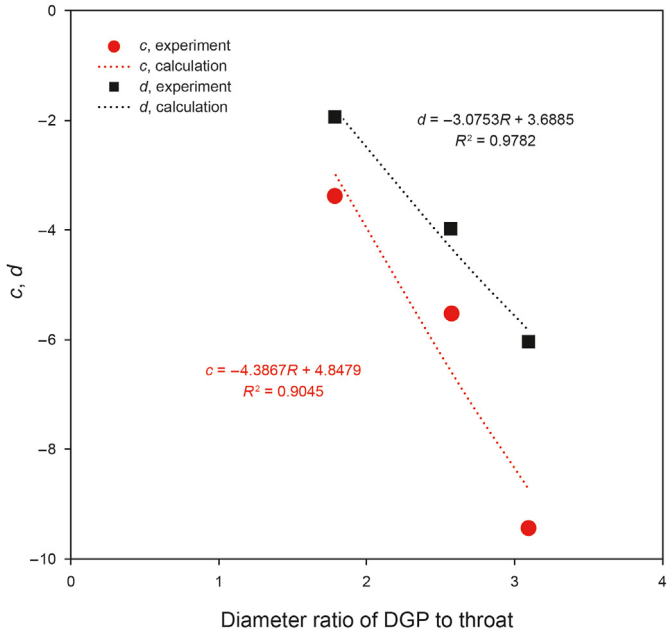

Fig. 14. The relationship between coefficients c, d and the diameter ratio of DGP to throat.

injection concentration and particle size, achieving the goal of deep reservoir plugging.

CRediT authorship contribution statement

Wen-Jing Zhao: Writing – original draft, Methodology, Investigation, Data curation. **Jing Wang:** Writing – review & editing, Methodology, Funding acquisition, Conceptualization. **Zhong-Yang Qi:** Visualization, Validation, Investigation. **Hui-Qing Liu:** Writing – review & editing, Project administration, Funding acquisition.

Declaration of competing interest

The authors declare that they have no known competing financial interests or personal relations that could have appeared to influence the work reported in this paper.

Acknowledgement

This work was supported by the Major National Science and Technology Project (No. 2016ZX05054011).

References

Bai, B., Wei, M., Liu, Y., 2013. Field and lab experience with a successful preformed particle gel conformance control technology. SPE Production and Operations

Symposium. https://doi.org/10.2118/164511-MS.
Bai, B.J., Liu, Y.Z., Coste, J.P., et al., 2007. Preformed particle gel for conformance control: transport mechanism through porous media. SPE Reservoir Eval. Eng. 10 (2), 176–184. https://doi.org/10.2118/89468-PA.
Bai, B.J., Zhou, J., Yin, M.F., 2015. A comprehensive review of polyacrylamide polymer gels for conformance control. Petrol. Explor. Dev. 42 (4), 525–532. https://doi.org/10.1016/S1876-3804(15)30045-8.
Elsharafi, M.O., Bai, B., 2013. Effect of strong preformed particle gel on unswept oil zones/areas during conformance control treatments. Ind. Eng. Chem. Res. 51 (35), 11547–11554. https://doi.org/10.1021/ie3007227.
Farasat, A., Younesian-Farid, H., Sadeghnejad, S., 2021. Conformance control study of preformed particle gels (PPGS) in mature waterflooded reservoirs: numerical and experimental investigations. J. Pet. Sci. Eng. 203, 108575–108588. https://doi.org/10.1016/j.petrol.2021.108575.
Feng, Q.H., Chen, X.C., Zhang, G., 2013. Experimental and numerical study of gel particles movement and deposition in porous media after polymer flooding. Transport Porous Media 97 (1), 67–85. https://doi.org/10.1007/s11242-012-0110-1.
Feng, Q.H., Cha, L.M., Dai, C.L., et al., 2020. Effect of particle size and concentration on the migration behavior in porous media by coupling computational fluid dynamics and discrete element method. Powder Technol. 360, 704–714. https://doi.org/10.1016/j.powtec.2019.10.011.
Guo, H., Lyu, X.Q., Xu, Y., et al., 2022. Recent advances of polymer flooding in China. In: SPE Conference at Oman Petroleum & Energy Show. https://doi.org/10.2118/200084-MS.
Herterich, J.G., Griffiths, I.M., Vella, D., et al., 2014. The effect of a concentration-dependent viscosity on particle transport in a channel flow with porous walls. AIChE J. 60 (5), 1891–1904. https://doi.org/10.1002/aic.14340.
Imqam, A., Bai, B.J., Ramadan, Al, et al., 2015. Preformed-particle-gel extrusion through open conduits during conformance-control treatments. SPE J. 20 (5), 1083–1093. https://doi.org/10.2118/169107-PA.
Imqam, A., Bai, B.J., Delshad, M., 2018. Micro-particle gel transport performance through unconsolidated sandstone and its blocking to water flow during conformance control treatments. Fuel 231, 479–488. https://doi.org/10.1016/j.fuel.2018.05.099.
Ji, W.J., Dai, C.L., Cao, Y.M., et al., 2023. A novel CO_2-resistant dispersed particle gel for gas channeling control in low-permeability reservoirs. J. Mol. Liq. 374, 121251–121261. https://doi.org/10.1016/j.molliq.2023.121251.
Kang, W., Kang, X., Lashari, Z.A., et al., 2021. Progress of polymer gels for conformance control in oilfield. Adv. Colloid Interface Sci. 289, 102363–102379. https://doi.org/10.1016/j.cis.2021.102363.
Liu, J.C., Almakimi, A., Wei, M.Z., et al., 2022. A comprehensive review of experimental evaluation methods and results of polymer micro/nanogels for enhanced oil recovery and reduced water production. Fuel 324, 124664–124684. https://doi.org/10.1016/j.fuel.2022.124664.
Liu, Y.G., Hou, J., Wang, Q.L., et al., 2017. Flow of preformed particle gel through porous media: a numerical simulation study based on the size exclusion theory. Ind. Eng. Chem. Res. 56 (10), 2840–2850. https://doi.org/10.1021/acs.iecr.6b03656.
Pi, Y.F., Liu, J.X., Cao, R.B., et al., 2023. Visualized study on a new preformed particle gels (PPG) + polymer system to enhance oil recovery by oil saturation monitoring online flooding experiment. Gels 9 (2), 81–99. https://doi.org/10.3390/gels9020081.
Pu, W.F., Du, D.J., Fan, H.C., et al., 2021. CO_2-responsive preformed gel particles with interpenetrating networks for controlling CO_2 breakthrough in tight reservoirs. Colloids Surf. A Physicochem. Eng. Asp. 613, 126065–126075. https://doi.org/10.1016/j.colsurfa.2020.126065.
Qiu, Y., Wei, M.Z., Bai, B.J., 2017. Descriptive statistical analysis for the ppg field applications in China: screening guidelines, design considerations, and performances. J. Pet. Sci. Eng. 153, 1–11. https://doi.org/10.1016/j.petrol.2017.03.030.
Sang, Q., Li, Y.J., Yu, L., et al., 2014. Enhanced oil recovery by branched-preformed particle gel injection in parallel-sandpack models. Fuel 136, 295–306. https://doi.org/10.1016/j.fuel.2014.07.065.
Seidy Esfahlan, M., Khodapanah, E., Tabatabaei-Nezhad, S.A., 2021. Comprehensive review on the research and field application of preformed particle gel conformance control technology. J. Pet. Sci. Eng. 202, 108440–108458. https://doi.org/10.1016/j.petrol.2021.108440.
Song, Z.J., Bai, B.J., Zhang, H., 2018. Preformed particle gel propagation and dehydration through semi-transparent fractures and their effect on water flow. J. Pet. Sci. Eng. 167, 549–558. https://doi.org/10.1016/j.petrol.2018.04.044.
Wang, J., Liu, H.Q., Wang, Z.L., et al., 2012. Experimental investigation on the filtering flow law of pre-gelled particle in porous media. Transport Porous Media 94 (1), 69–86. https://doi.org/10.1007/s11242-012-9988-x.
Wang, J., Liu, H.Q., Wang, Z.L., et al., 2013. Numerical simulation of preformed particle gel flooding for enhancing oil recovery. J. Pet. Sci. Eng. 112, 248–257. https://doi.org/10.1016/j.petrol.2013.11.011.
Wang, J., Liu, H.Q., Zhang, H.l., Sepehrnoori, K., 2017a. Simulation of deformable preformed particle gel propagation in porous media. AIChE J. 63 (10), 4628–4641. https://doi.org/10.1002/aic.15793.
Wang, J., Zhang, H.L., Liu, H.Q., et al., 2017b. Quantification of transportation of deformable gel particles in porous media. In: SPE Annual Technical Conference and Exhibition. https://doi.org/10.2118/187266-MS.
Wang, X.Y., Gong, L., Li, Y., et al., 2023. Developments and applications of the cfd-dem method in particle–fluid numerical simulation in petroleum engineering: a review. Appl. Therm. Eng. 222, 119865–119882. https://doi.org/10.1016/j.applthermaleng.2022.119865.
Wang, Z., Bai, B.J., 2018. Preformed-particle-gel placement and plugging performance in fractures with tips. SPE J. 23 (6), 2316–2326. https://doi.org/10.2118/193997-PA.
Wang, Z., Bai, B.J., Zhou, E.Z., et al., 2019. Experimental evaluation of oxidizing breakers for a polyacrylamide-based re-crosslinkable preformed particle gel. Energy Fuels 33 (6), 5001–5010. https://doi.org/10.1021/acs.energyfuels.9b00709.
Wei, B., Hou, J., Sukop, M.C., et al., 2019. Pore scale study of amphiphilic fluids flow using the lattice Boltzmann model. Int. J. Heat Mass Transf. Pergamon. 139, 725–735. https://doi.org/10.1016/j.ijheatmasstransfer.2019.05.056.
Wu, D.J., Zhou, K., Hou, J., et al., 2020. Review of experimental and simulation studies of enhanced oil recovery using viscoelastic particles. J. Dispersion Sci. Technol. 42 (7), 956–969. https://doi.org/10.1080/01932691.2020.1723620.
Yang, H.B., Zhou, B.B., Zhu, T.Y., et al., 2021. Conformance control mechanism of low elastic polymer microspheres in porous medium. J. Pet. Sci. Eng. 196, 107708–107717. https://doi.org/10.1016/j.petrol.2020.107708.
Yao, C.J., Lei, G.L., Gao, X.M., et al., 2013. Controllable preparation, rheology, and plugging property of micron-grade polyacrylamide microspheres as a novel profile control and flooding agent. J. Appl. Polym. Sci. 130 (2), 1124–1130. https://doi.org/10.1002/app.39283.
Yuan, C.D., Pu, W.F., Varfolomeev, M.A., et al., 2021. Deformable microgel for enhanced oil recovery in high-temperature and ultrahigh-salinity reservoirs: how to design the particle size of microgel to achieve its optimal match with pore throat of porous media. SPE J. 26 (4), 2053–2067. https://doi.org/10.2118/197804-PA.
Zhang, X., Deng, J.N., Yang, K., et al., 2022. High-strength and self-degradable sodium alginate/polyacrylamide preformed particle gels for conformance control to enhance oil recovery. Petrol. Sci. 19 (6), 3149–3158. https://doi.org/10.1016/j.petsci.2022.06.012.
Zhao, M.W., Yan, X.W., Wang, X.Y., et al., 2023a. The development of a smart gel for CO_2 mobility control in heterogeneity reservoir. Fuel 342, 127844–127853. https://doi.org/10.1016/j.fuel.2023.127844.
Zhao, S., Pu, W.F., Wei, B., et al., 2019. A comprehensive investigation of polymer microspheres (PMS) migration in porous media: EOR implication. Fuel 235, 249–258. https://doi.org/10.1016/j.fuel.2018.07.125.
Zhao, W.J., Wang, J., Qian, Q.H., et al., 2023b. Evolution law of dominant flow channels of water flooding in heterogeneous reservoir. Fault-Block Oil Gas Field 30 (5), 847–857. https://doi:10.6056/dkyqt202305018 (in Chinese).
Zhao, Y., Leng, J.Q., Lin, B.H., et al., 2021. Experimental study of microgel conformance-control treatment for a polymer-flooding reservoir containing superpermeable channels. SPE J. 26 (4), 2305–2317. https://doi.org/10.2118/205486-PA.
Zhao, Y., Bai, B., 2022. Experimental study of transport behavior of swellable microgel particles in superpermeable channels for conformance control. SPE J. 27 (1), 790–805. https://doi.org/10.2118/208576-PA.
Zhou, K., Hou, J., Zhang, X.S., et al., 2013. Optimal control of polymer flooding based on simultaneous perturbation stochastic approximation method guided by finite difference gradient. Comput. Chem. Eng. 55 (2013), 40–49. https://doi.org/10.1016/j.compchemeng.2013.04.009.
Zhou, K., Hou, J., Sun, Q.C., et al., 2017. An efficient LBM-DEM simulation method for suspensions of deformable preformed particle gels. Chem. Eng. Sci. 167, 288–296. https://doi.org/10.1016/j.ces.2017.04.026.
Zhou, K., Hou, J., Sun, Q.C., et al., 2019. Study on the flow resistance of the dispersion system of deformable preformed particle gel in porous media using LBM-DEM-IMB method. J. Dispersion Sci. Technol. 40 (10), 1523–1530. https://doi.org/10.1080/01932691.2019.1645028.